Microscopic theory of quantum anomalous Hall effect in graphene

Zhenhua Qiao,[1] Hua Jiang,[2] Xiao Li,[1] Yugui Yao,[3] and Qian Niu[1,2]
[1]*Department of Physics, University of Texas at Austin, Austin, Texas 78712, USA*
[2]*International Center for Quantum Materials, Peking University, Beijing 100871, China*
[3]*School of Physics, Beijing Institute of Technology, Beijing 100081, China*
(Received 2 January 2012; revised manuscript received 15 March 2012; published 27 March 2012)

We present a microscopic theory to give a physical picture of the formation of the quantum anomalous Hall (QAH) effect in magnetized graphene coupled with Rashba spin-orbit coupling. Based on a continuum model at valley K or K', we show that there exist two distinct physical origins of the QAH effect at two different limits. For large exchange field M, the quantization of Hall conductance in the absence of Landau-level quantization can be regarded as a summation of the topological charges carried by skyrmions from real-spin textures and merons from AB sublattice pseudospin textures, while for strong Rashba spin-orbit coupling λ_R, the four-band low-energy model Hamiltonian is reduced to a two-band extended Haldane model, giving rise to a nonzero Chern number $\mathcal{C} = 1$ at either K or K'. In the presence of staggered AB sublattice potential U, a topological phase transition occurs at $U = M$ from a QAH phase to a quantum valley Hall phase. We further find that the band gap responses at K and K' are different when λ_R, M, and U are simultaneously considered. We also show that the QAH phase is robust against weak intrinsic spin-orbit coupling λ_{SO}, and it transitions to a trivial phase when $\lambda_{SO} > (\sqrt{M^2 + \lambda_R^2} + M)/2$. Moreover, we use a tight-binding model to reproduce the *ab initio* method obtained band structures through doping magnetic atoms on 3×3 and 4×4 supercells of graphene, and explain the physical mechanisms of opening a nontrivial bulk gap to realize the QAH effect in different supercells of graphene.

DOI: 10.1103/PhysRevB.85.115439 PACS number(s): 73.43.−f, 72.20.−i, 73.22.Pr, 75.50.Pp

I. INTRODUCTION

In 1879, Edward H. Hall discovered that when an electric field flows through a conductor in the presence of a perpendicular magnetic field, charge carriers subjected to the Lorentz force are pushed to one side of the conductor. At equilibrium, the carrier accumulation generates a transverse bias to balance the Lorentz force. This is the famous "Hall effect". In two-dimensional electron systems, the quantized version of the Hall effect was observed due to Landau quantization,[1] which is characterized by a precisely quantized Hall conductance, i.e., $\sigma_{xy} = \mathcal{C}e^2/h$, where $\mathcal{C}$ is known as the TKNN number or Chern number.[2,3]

To produce a Hall effect, breaking time-reversal symmetry is an essential condition. In addition to magnetic field, an internal magnetization coupled with spin-orbit coupling could also give rise to the Hall effect. To distinguish this from the ordinary Hall effect, this magnetization-induced one was called the "anomalous" Hall effect. Although it has been experimentally observed for over a century, the physical origin of the anomalous Hall effect is still unclear. In general, the mechanism of the anomalous Hall effect is classified as extrinsic or intrinsic according to its origins. The extrinsic one arises from the spin-dependent scattering impurities, while the latter one can be expressed in terms of Berry-phase curvatures in the crystal momentum space.[4]

Similar to the quantization of the ordinary Hall effect, the anomalous Hall effect was also predicted to be quantized by Haldane in a honeycomb lattice toy model with vanishing magnetic field.[5] Subsequently, other proposals were made toward the realization of the quantum anomalous Hall (QAH) effect, i.e., in mercury-based quantum wells,[6] disorder-induced Anderson insulators,[7] optical lattices,[8] and magnetic topological insulators.[9] Despite the theoretical progress, the QAH effect has not been observed experimentally. In a recent paper,[10,11] we found that graphene shows great potential to host the long-sought QAH state in the presence of Rashba spin-orbit coupling and exchange field. Based on the state-of-the-art first-principles calculation method, researchers[12,13] further demonstrated that this QAH phase could be engineered via doping $3d$ or $5d$ transition-metal atoms on the hollow sites of graphene. The final realization of the QAH effect will enable the application of novel quantum devices due to the dissipationless nature.

In this paper, we demonstrate a microscopic theory to study the physical origins of the QAH effect in graphene due to the presence of both Rashba spin-orbit coupling and exchange using a low-energy continuum model. In the limit of strong exchange field and weak Rashba spin-orbit coupling, the quantization of the Hall conductance should be attributed to the real-spin texture-induced skyrmions and AB sublattice pseudospin texture-induced merons, while in the other limit, i.e., weak exchange field and strong Rashba spin-orbit coupling, the four-band low-energy model can be reduced to a two-band extended Haldane model. We also show that this QAH phase is robust against weak staggered AB sublattice potentials or intrinsic spin-orbit coupling, which is present in real materials. Using a tight-binding method, we reproduce all the *ab initio* obtained band structures of doping magnetic atoms in 3×3 or 4×4 supercells of graphene. And we give an explanation of the formation mechanism of the QAH effect in 3×3 or 4×4 supercell of graphene.

The remainder of the paper is organized as follows. In Sec. II, we present tight-binding and continuum models of graphene in the presence of Rashba spin-orbit coupling, intrinsic spin-orbit coupling, exchange field, and staggered AB sublattice potential. Section III discusses the physical

origin of the quantum anomalous Hall effect in graphene at two different limits using a continuum model. In Sec. IV, we show the robustness of the quantum anomalous Hall state in the presence of either staggered AB sublattice potential or intrinsic spin-orbit coupling. In Sec. V, we use a tight-binding model to explain a recent *ab initio* work about realizing the quantum anomalous Hall effect in 3×3 and 4×4 supercell of graphene. A brief summary is given in Sec. VI to close the paper.

II. MODEL HAMILTONIAN OF GRAPHENE

The real-space π-orbital tight-binding Hamiltonian of single-layer graphene in the presence of uniformly distributed Rashba or intrinsic spin-orbit coupling, exchange field, and staggered AB sublattice potentials is written as[10,14,15]

$$H = H_0 + H_R + H_{SO} + H_M + H_U, \tag{1}$$

where each term is given by

$$\begin{aligned}
H_0 &= -t \sum_{\langle ij\rangle;\alpha} c^\dagger_{i\alpha} c_{j\alpha};\\
H_R &= it_R \sum_{\langle ij\rangle;\alpha,\beta} \hat{\mathbf{e}}_z \cdot (s_{\alpha\beta} \times \mathbf{d}_{ij}) c^\dagger_{i\alpha} c_{j\beta};\\
H_{SO} &= \frac{2i}{\sqrt{3}} t_{SO} \sum_{\ll ij \gg} c^\dagger_i \boldsymbol{s} \cdot (\mathbf{d}_{kj} \times \mathbf{d}_{ik}) c_j;\\
H_M &= M \sum_{i;\alpha,\beta} c^\dagger_{i\alpha} s^z_{\alpha\beta} c_{i\beta};\\
H_U &= \sum_{i;\alpha} c^\dagger_{i\alpha} V_i c_{i\alpha}.
\end{aligned}$$

Here, $c^\dagger_{i\alpha}$ and $c_{i\alpha}$ are π-orbital creation and annihilation operators for an electron with spin α on site i. The first term H_0 represents the nearest-neighbor hopping with amplitude $t = 2.6$ eV. The second term H_R describes the Rashba spin-orbit coupling with $\mathbf{d}_{ij}$ being a lattice vector pointing from site j to site i. The third term H_{SO} is the intrinsic spin-orbit coupling with k connecting the next-nearest neighbor sites i and j. $\langle\rangle$ ($\ll\gg$) runs over all the nearest (next-nearest) neighbor hopping sites. The fourth term and the last term correspond to the exchange field and staggered AB-sublattice potentials, respectively. We set $V_i = +U$ at A-type sublattices and $V_i = -U$ at B-type sublattices. α and β denote spin indices, and $\boldsymbol{s}$ are the spin Pauli matrices.

By performing a Fourier transformation, the real-space Hamiltonian in Eq. (1) is converted to a 4×4 matrix $H(\boldsymbol{k})$ in the momentum space. In this paper, we choose the lattice unit vectors to be

$$\boldsymbol{a}_1 = \frac{a}{2}(2\sqrt{3},0), \quad \boldsymbol{a}_2 = \frac{a}{2}(\sqrt{3},3), \tag{2}$$

and the corresponding reciprocal-lattice vectors are given by

$$\boldsymbol{b}_1 = \frac{2\pi}{a}\left(\frac{1}{\sqrt{3}}, \frac{-1}{3}\right), \quad \boldsymbol{b}_2 = \frac{2\pi}{a}\left(0, \frac{2}{3}\right), \tag{3}$$

where $a = 1.42$ Å is the distance between nearest-neighbor carbon-carbon atoms, and we set a to be unity in the following calculation for simplicity. On the basis of $\{\psi_{A\uparrow}, \psi_{A\downarrow}, \psi_{B\uparrow}, \psi_{B\downarrow}\}$, the corresponding momentum-space Hamiltonian of each term is listed in the following.

(A) Nearest-neighbor hopping term:

$$H_0(\boldsymbol{k}) = -t \begin{bmatrix} 0 & \gamma_0 \\ \gamma_0^* & 0 \end{bmatrix}, \tag{4}$$

with

$$\begin{aligned}
\gamma_0 = \Bigg[&\left(2\cos\frac{\sqrt{3}k_x}{2}\cos\frac{k_y}{2} + \cos k_y\right)\\
&+ i\left(2\cos\frac{\sqrt{3}k_x}{2}\sin\frac{k_y}{2} - \sin k_y\right)\Bigg]\mathbf{1}_s,
\end{aligned}$$

where $\mathbf{1}_s$ is a 2×2 identity matrix.

(B) Rashba spin-orbit coupling term:

$$H_R(\boldsymbol{k}) = t_R \begin{bmatrix} 0 & \gamma_R \\ \gamma_R^* & 0 \end{bmatrix}, \tag{5}$$

with

$$\begin{aligned}
\gamma_R = \Bigg[&\left(\cos\frac{\sqrt{3}k_x}{2}\sin\frac{k_y}{2} + \sin k_y\right)\\
&- i\left(\cos\frac{\sqrt{3}k_x}{2}\cos\frac{k_y}{2} - \cos k_y\right)\Bigg] s_x\\
&- \sqrt{3}\sin\frac{\sqrt{3}k_x}{2}\left(i\sin\frac{k_y}{2} + \cos\frac{k_y}{2}\right) s_y.
\end{aligned}$$

(C) Intrinsic spin-orbit coupling term:

$$H_{SO}(\boldsymbol{k}) = t_{SO} \begin{bmatrix} \gamma_{SO} & 0 \\ 0 & -\gamma_{SO} \end{bmatrix}, \tag{6}$$

where

$$\gamma_{SO} = -4t_{SO}\sin\frac{\sqrt{3}k_x}{2}\left(\cos\frac{3k_y}{2} - \cos\frac{\sqrt{3}k_x}{2}\right) s_z.$$

(D) Exchange field term:

$$H_M(\boldsymbol{k}) = M \begin{bmatrix} s_z & 0 \\ 0 & s_z \end{bmatrix}. \tag{7}$$

(E) Staggered AB sublattice potential term:

$$H_U(\boldsymbol{k}) = U \begin{bmatrix} \mathbf{1}_s & 0 \\ 0 & -\mathbf{1}_s \end{bmatrix}. \tag{8}$$

By directly diagonalizing $H(\boldsymbol{k})$ at each crystal momentum $\boldsymbol{k}$, one can easily obtain the bulk band structure. As reported in a recent paper,[10] we found that a nontrivial bulk gap opens when both the Rashba spin-orbit coupling t_R and exchange field M are considered simultaneously. Through calculating the Chern number by integrating the Berry curvatures in the first Brillouin zone, we found that the resulting Chern number is nonzero, indicating a quantum anomalous Hall state. The central issue in this paper is to give a physical picture to understand the formation of this nontrivial state. Therefore, study of the low-energy effective model is required.

Through expanding the tight-binding Hamiltonian in Eqs. (4) to (8) at the vicinity of valleys K and K', i.e., $(k_x,k_y) = (\pm 4\pi/3\sqrt{3},0)$, the low-energy effective model Hamiltonian of each term at valleys K and K' is summarized as follows on the basis of $\{\psi_{A\uparrow}, \psi_{A\downarrow}, \psi_{B\uparrow}, \psi_{B\downarrow}\}$:

$$h_0(\boldsymbol{k}) = v(\eta\sigma_x k_x + \sigma_y k_y)\mathbf{1}_s; \tag{9}$$

$$h_R(\boldsymbol{k}) = \frac{\lambda_R}{2}(\eta\sigma_x s_y - \sigma_y s_x); \tag{10}$$

$$h_{SO}(\boldsymbol{k}) = \eta\lambda_{SO}\sigma_z s_z; \tag{11}$$

$$h_M(\boldsymbol{k}) = M\mathbf{1}_\sigma s_z; \tag{12}$$

$$h_U(\boldsymbol{k}) = U\sigma_z\mathbf{1}_s. \tag{13}$$

Here, $\eta = \pm 1$ labels valley degrees of freedom; $\boldsymbol{\sigma}$ are Pauli matrices representing the AB-sublattice pseudospin degrees of freedom. The Fermi velocity, Rashba spin-orbit coupling, and intrinsic spin-orbit coupling are given by $v = 3t/2$, $\lambda_R = 3t_R$, and $\lambda_{SO} = 3\sqrt{3}t_{SO}$, respectively.

One should note that the present tight-binding model in the presence of uniformly distributed parameters is mainly of academic importance and difficult to be realized in experiment. To demonstrate the possibility of our proposal, we have employed the first-principles calculation method to investigate the electronic properties through doping $3d$ transition-metal atoms on 3×3 and 4×4 supercells of graphene. And it is reported that though the inducing Rashba spin-orbit coupling and exchange field are nonuniformly distributed in the supercells, they result in exactly the same quantum anomalous Hall state and share the same spirit as those in the theoretical model with uniform Rashba spin-orbit coupling and exchange field.[12] In Sec. V, we will present a tight-binding model to simulate doping magnetic atoms on 3×3 and 4×4 supercells of graphene.

III. PHYSICAL ORIGIN OF QUANTUM ANOMALOUS HALL EFFECT

When the Rashba spin-orbit coupling λ_R and exchange field M are taken into account simultaneously, the continuum model Hamiltonian is

$$H(\boldsymbol{k}) = h_0(\boldsymbol{k}) + h_R(\boldsymbol{k}) + h_M(\boldsymbol{k}). \tag{14}$$

In Refs. 10 and 11, we have pointed out that a nontrivial bulk band gap opens up as long as λ_R and M are nonzero. Based on the Kubo formula, when the Fermi energy lies within the bulk band gap, the corresponding Hall conductance σ_{xy} is shown to be quantized as

$$\sigma_{xy} = \mathcal{C}\frac{e^2}{h}, \tag{15}$$

where the Chern number is $\mathcal{C} = 2\mathrm{sgn}(M)$ and can be calculated from

$$\mathcal{C} = \frac{1}{2\pi}\sum_{K,K'}\sum_{n=1,2}\int_{-\infty}^{+\infty} dk_x dk_y \Omega_n(k_x,k_y). \tag{16}$$

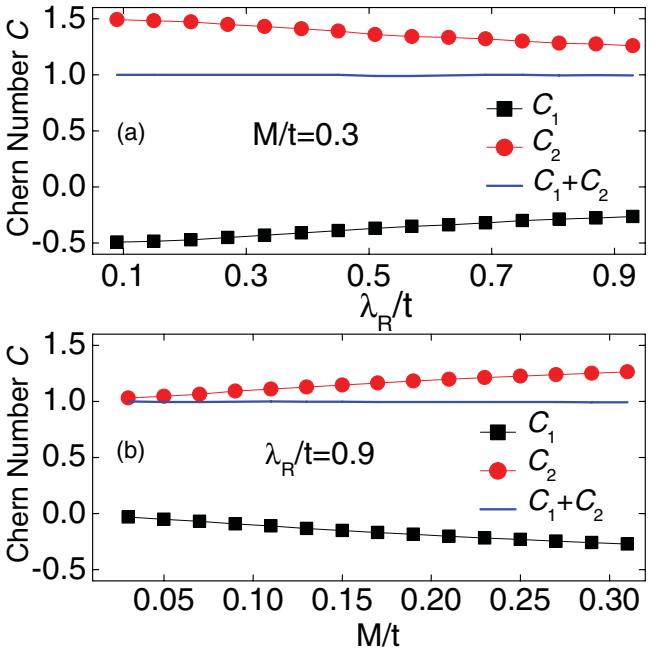

FIG. 1. (Color online) (a) Chern number of each valence band as a function of Rashba spin-orbit coupling λ_R at fixed exchange field $M/t = 0.3$. (b) Chern number of each valence band as a function of exchange field M at fixed Rashba spin-orbit coupling $\lambda_R/t = 0.9$. The solid (blue) line represents the summation of the two valence bands. The cutoff of k_x and k_y is set to be $k_0 = \pi/2a$.

The sum is taken over both valley K or K' and n occupied valence bands below the bulk band gap. Ω_n is the momentum-space Berry curvature of the nth band and can be obtained through the formula

$$\Omega_n(\boldsymbol{k}) = -\sum_{n'\neq n}\frac{2\mathrm{Im}\langle\psi_{n\boldsymbol{k}}|v_x|\psi_{n'\boldsymbol{k}}\rangle\langle\psi_{n'\boldsymbol{k}}|v_y|\psi_{n\boldsymbol{k}}\rangle}{(\omega_{n'}-\omega_n)^2}, \tag{17}$$

where $\omega_n \equiv E_n/\hbar$, and $v_{x(y)}$ is the Fermi velocity operator.

It is already known that the Chern numbers of valleys K and K' are equal;[11] i.e., $\mathcal{C}_K = \mathcal{C}_{K'} = 1$. However, the component from each valence band is still unclear. For clarity, we label the lowest valence band as the 1st band, and the other one close to the bulk band gap as the 2nd band. Figure 1 plots the Chern number of each band and the total Chern number as functions of exchange field M and Rashba spin-orbit coupling λ_R. In Fig. 1(a), the exchange field is fixed at $M/t = 0.3$. We find that, for extremely small Rashba spin-orbit coupling $\lambda_R \to 0$, the Chern number of the 1st valence band is half quantized with a negative sign, i.e., $\mathcal{C}_1 = -0.5$, and that of the 2nd valence band is one and half quantized, i.e., $\mathcal{C}_2 = 1.5$. When Rashba spin-orbit coupling λ_R gradually increases, the absolute values of $\mathcal{C}_1$ and $\mathcal{C}_2$ are both reduced. On the contrary, in Fig. 1(b) Rashba spin-orbit coupling is fixed to be $\lambda_R/t = 0.3$. One observes that for extremely weak exchange field $M \to 0$, the 1st valence band gives no contribution to the total Chern number; i.e., $\mathcal{C}_1 = 0$ and $\mathcal{C}_2 = 1$. Along with the increasing of the exchange field, $\mathcal{C}_1$ increases with a

negative sign while $\mathcal{C}_2$ is also linearly increased, keeping the total Chern number quantized to be $\mathcal{C} = 1$.

Based on the analysis of the Chern number response at the two different limits, i.e., $M/\lambda_R \gg 1$ and $\lambda_R/M \gg 1$, one can imagine that the resulting Hall conductance quantization should correspond to different formation mechanisms. In the following, we give a clear understanding of the physical origins of the quantum anomalous Hall effect at the two different limits.

A. $M/\lambda_R \gg 1$ limit: skyrmion and meron

From Fig. 1(a), one can note that both valence bands contribute to the total Hall conductance; therefore the four-band Hamiltonian cannot be reduced to a two-band effective Hamiltonian model. In the following, we study the origin of the Hall conductance from each band. In our studied single-layer graphene system, there are two kinds of spin degrees of freedom: real-spin $\boldsymbol{s}$ and AB sublattice pseudospin $\boldsymbol{\sigma}$. On the basis of $\{\psi_{A\uparrow}, \psi_{A\downarrow}, \psi_{B\uparrow}, \psi_{B\downarrow}\}$, the real-spin and pseudospin components can be evaluated through

$$\begin{aligned} \langle \boldsymbol{s}_i \rangle &= \langle \psi | \mathbf{1}_\sigma \otimes \boldsymbol{s}_i | \psi \rangle, \\ \langle \boldsymbol{\sigma}_i \rangle &= \langle \psi | \boldsymbol{\sigma}_i \otimes \mathbf{1}_s | \psi \rangle, \end{aligned} \tag{18}$$

where $i = \{x, y, z\}$, and $|\psi\rangle$ is a 4×1 eigenvector.

In Fig. 2, we exhibit the spin textures of the real-spin and AB sublattice pseudospin at valleys K and K' for the two valence bands below the bulk band gap, respectively. One can observe that the real-spin textures of the two valence bands of valley K are exactly the same as that of valley K' [see Figs. 2(a)–2(d)]; i.e., for the 1st band the spins are uniformly pointing toward the south pole in the whole momentum space, contributing nothing to the total Chern number, while for the 2nd band the spins close to valleys K and K' point toward the south pole whereas those far away from the center point toward the opposite north pole (note that there should exist a circular region with spin lying within the in-plane of the equator), which phenomenally corresponds to a skyrmion that contributes to one topological charge.[16]

However, it becomes more complicated for the AB sublattice pseudospin textures [see Figs. 2(e)–2(h)]. For valley K, one can see that the in-plane pseudospin components of both valence bands point toward the center with the same winding pattern, the out-of-plane pseudospin components close to the center point toward either the south pole (1st band) or north pole (2nd band), but those far away from the center are vanishing. For valley K', one finds that the pseudospin textures are distinct from those at valley K. For example, the in-plane pseudospins point toward the center without any winding, while the out-of-plane pseudospins only exist near the valleys and point to either the north pole (1st band) or south pole (2nd band). All these suggest that each of the four different pseudospin textures correspond to a meron, i.e., half skyrmion.[17]

To confirm the above analysis, we should precisely calculate the Chern number (or topological charge) resulting from each special real-spin or pseudospin texture using the formula

$$n = \frac{1}{4\pi} \int\int dk_x dk_y (\partial_{k_x} \hat{\boldsymbol{h}} \times \partial_{k_y} \hat{\boldsymbol{h}}) \cdot \hat{\boldsymbol{h}}, \tag{19}$$

where n is a topological charge counting the number of times a unit vector $\hat{\boldsymbol{h}}(k)$ winding around the unit sphere as a function of $\boldsymbol{k}$. $\hat{\boldsymbol{h}}(\boldsymbol{k}) \equiv \boldsymbol{h}(\boldsymbol{k})/|\boldsymbol{h}(\boldsymbol{k})|$ with $\boldsymbol{h}(\boldsymbol{k})$ representing the projection of the Hamiltonian shown in Eq. (14) into the real-spin or pseudospin space. For $M/\lambda_R \gg 1$, our numerical calculation shows that

$$n_{1s}^K = n_{1s}^{K'} = 0; \tag{20}$$

$$n_{2s}^K = n_{2s}^{K'} \simeq 1.0; \tag{21}$$

$$n_{1\sigma}^K = n_{1\sigma}^{K'} \simeq -0.5; \tag{22}$$

$$n_{2\sigma}^K = n_{2\sigma}^{K'} \simeq 0.5. \tag{23}$$

Therefore the corresponding Chern numbers become

$$\mathcal{C}_1^K = n_{1s}^K + n_{1\sigma}^K = -0.5; \tag{24}$$

$$\mathcal{C}_1^{K'} = n_{1s}^{K'} + n_{1\sigma}^{K'} = -0.5; \tag{25}$$

$$\mathcal{C}_2^K = n_{2s}^K + n_{2\sigma}^K = 1.5; \tag{26}$$

$$\mathcal{C}_2^{K'} = n_{2s}^{K'} + n_{2\sigma}^{K'} = 1.5; \tag{27}$$

$$\mathcal{C}^K = \mathcal{C}_1^K + \mathcal{C}_2^K = 1; \tag{28}$$

$$\mathcal{C}^{K'} = \mathcal{C}_1^{K'} + \mathcal{C}_2^{K'} = 1. \tag{29}$$

From the relationship shown in Eqs. (22) and (23), one can find that though the spins point to opposite poles (for example, see the pseudospin textures of the 1st valence band at K and K'), their different winding patterns give rise to the same winding number.

Therefore, in the limit of $M/\lambda_R \gg 1$, the formation of the quantum anomalous Hall state originates from both skyrmions carried by the real-spin textures and merons carried by the AB sublattice pseudospin textures. Quantitatively, the pseudospin-induced topological charges n from 1st and 2nd valence are exactly opposite to cancel each other, which makes the real-spin-induced skyrmions from 2nd become the only source to achieve the quantized Hall conductance without external magnetic field.

B. $\lambda_R/M \gg 1$ limit: an extended Haldane model

In the limit of strong Rashba spin-orbit coupling λ_R and weak exchange field M, the total Chern number mainly comes from the 2nd valence band while the contribution from 1st valence band is negligible as shown in Fig. 1(b); i.e., $\mathcal{C}_1 \simeq 0$ and $\mathcal{C}_2 \simeq 1$. This indicates that it is possible to obtain a reduced effective two-band model Hamiltonian through disregarding the high-energy bands. By reconstructing the basis to be $\{\psi_{A\uparrow}, \psi_{B\downarrow}, \psi_{B\uparrow}, \psi_{A\downarrow}\}$, the continuum Hamiltonian at valley K is

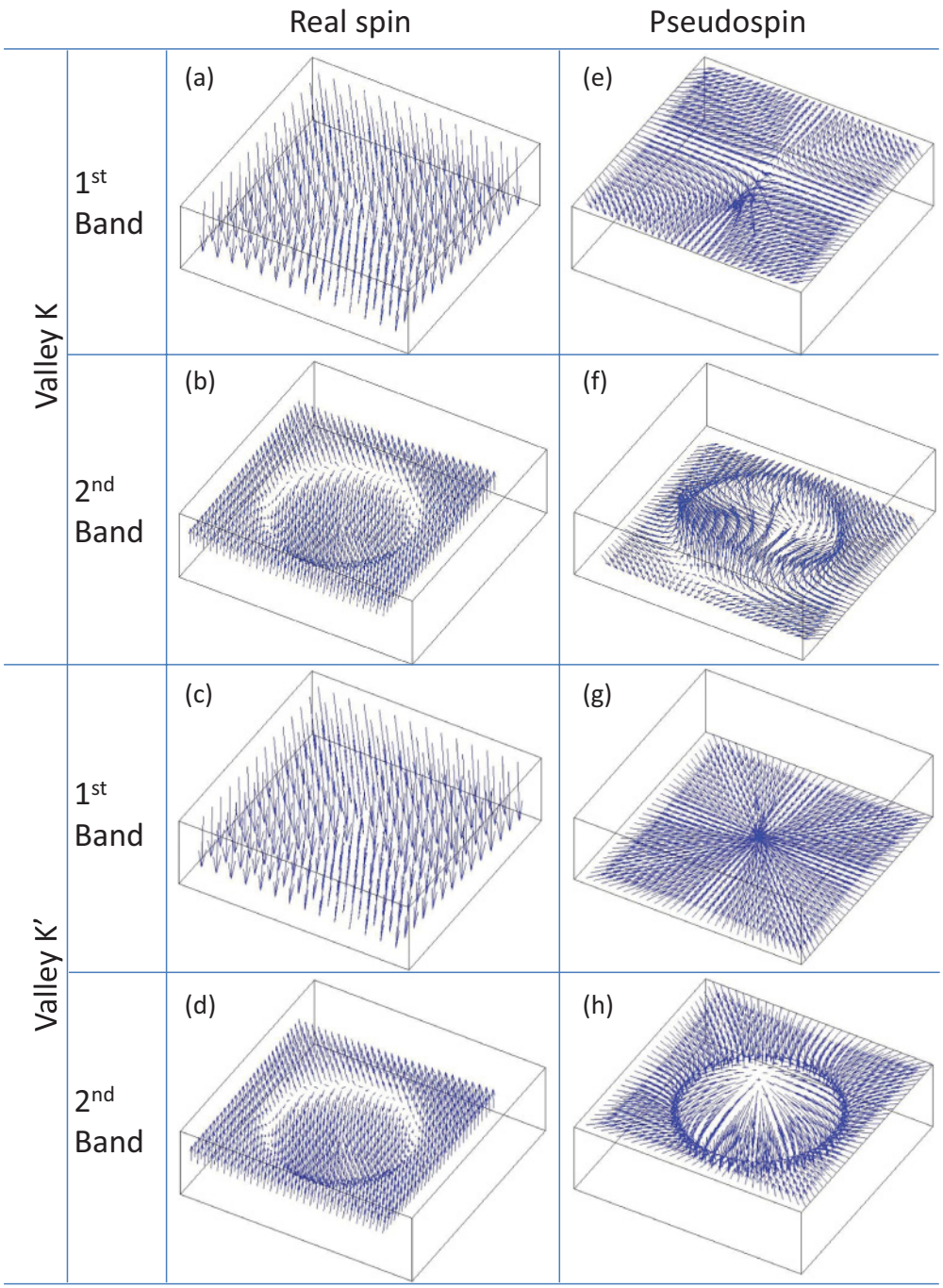

FIG. 2. (Color online) Real-spin and pseudospin textures of the two valence bands of graphene below the band gap at valleys K and K' in the limit of $M/\lambda_R \gg 1$ (here, we set $M = 0.8$ and $\lambda_R = 0.12$). (a)–(d): Real-spin textures of the 1st and 2nd valence bands at valleys K and K'. (a) and (c): Spins point toward the south pole uniformly. (b) and (d): Spins at the center point toward the south pole while those far away from the center point toward the north pole, which indicates a skyrmion. (e)–(h): Pseudospin textures of the 1st and 2nd valence bands at valleys K and K'. (e) and (f): In-plane pseudospin components share the similar winding pattern pointing toward the center, but out-of-plane pseudospin components point toward south and north poles, respectively. (g) and (h): In-plane pseudospin components point toward the center without any winding, while out-of-plane pseudospin components point toward north and south poles, respectively. Each pseudospin texture corresponds to a meron or half skyrmion.

written as

$$H_K = \begin{bmatrix} M & 0 & vk_- & 0 \\ 0 & -M & 0 & vk_+ \\ vk_+ & 0 & M & -i\lambda_R \\ 0 & vk_- & i\lambda_R & -M \end{bmatrix} = \begin{bmatrix} H_1 & T \\ T^* & H_2 \end{bmatrix},$$

where H_1 and H_2 represent the two block Hamiltonians on the basis of $(\psi_{A\uparrow}, \psi_{B\downarrow})$ and $(\psi_{B\uparrow}, \psi_{A\downarrow})$, respectively; T couples the two different blocks. At the vicinity of K, H_1 and H_2 correspond to the low-energy band (i.e., $\varepsilon = \pm M$) and high-energy band (i.e., $\varepsilon = \pm\sqrt{M^2 + \lambda_R^2}$), and the coupling T becomes extremely weak. Therefore, an effective Hamiltonian

can be obtained to describe the low-energy physics at the K point:

$$\begin{aligned} H_{\rm eff}^{K} &\simeq H_1 - T H_2^{-1} T^* = d_z\sigma_z + d_y\sigma_y + d_x\sigma_x, \\ d_z &= M\left(1 - \frac{v^2}{\lambda_R^2}k^2\right), \\ d_y &= -\frac{v^2}{\lambda_R}\left(k_x^2 - k_y^2\right), \\ d_x &= 2\frac{v^2}{\lambda_R}k_x k_y. \end{aligned} \tag{30}$$

Similarly, after reconstructing the basis to be $\{\psi_{B\uparrow}, \psi_{A\downarrow}, \psi_{A\uparrow}, \psi_{B\downarrow}\}$, the continuum Hamiltonian at valley K' becomes

$$H_{K'} = \begin{bmatrix} M & 0 & -vk_- & 0 \\ 0 & -M & 0 & -vk_+ \\ -vk_+ & 0 & M & i\lambda_R \\ 0 & -vk_- & -i\lambda_R & -M \end{bmatrix} = \begin{bmatrix} H_1 & -T \\ -T^* & H_2^* \end{bmatrix}.$$

Using a similar method in Eq. (30), we can obtain the reduced effective two-band model Hamiltonian at the vicinity of K':

$$H_{\rm eff}^{K'} \simeq H_1 - T(H_2^*)^{-1}T^* = d_z\sigma_z - d_y\sigma_y - d_x\sigma_x. \tag{31}$$

Through comparing the obtained effective Hamiltonian at K or K' in Eqs. (30) and (31) with the famous Haldane toy model in Ref. 5, we find that they share a similar characteristic form. Especially, when $k^2 > \lambda_R^2/v^2$, the coefficient of d_z can change its sign from positive to negative. This signals that the reduced effective Hamiltonians are definitely extended Haldane models exhibiting a nonzero Chern number. Since the sign is directly related to d_z and d_z is an odd (even) function with respect to M (λ_R), the sign of the resulting quantum Hall conductance should only be dependent on M. Moreover, the coefficient of σ_z in Eq. (31) is exactly the same as that in Eq. (30). Therefore, according to Eq. (19) both effective Hamiltonians at K and K' give rise to the same Chern number; thus the total Chern number is $\mathcal{C} = 2\text{sgn(M)}$.

IV. ROBUSTNESS OF QUANTUM ANOMALOUS HALL EFFECT

A. Staggered AB sublattice potential

When graphene is doped with some magnetic atoms on top of carbon atoms, i.e., one adatom sitting on top of the carbon atom in a 4×4 or 5×5 supercell of graphene, besides the magnetic proximity-induced exchange field and the interaction-induced Rashba spin-orbit coupling, the imbalanced AB sublattice potentials may also be introduced.[12] In the following, we address the possible effect of the staggered AB sublattice potentials on the quantum anomalous Hall state. In the low-energy limit, the effective Hamiltonian in the presence of Rashba spin-orbit coupling λ_R, exchange field M and staggered sublattice potential U on the basis of $\{\psi_{A\uparrow}, \psi_{A\downarrow}, \psi_{B\uparrow}, \psi_{B\downarrow}\}$ is written as

$$H(\boldsymbol{k}) = h_0(\boldsymbol{k}) + h_R(\boldsymbol{k}) + h_M(\boldsymbol{k}) + h_U(\boldsymbol{k}). \tag{32}$$

After a direct diagonalization of the above Hamiltonian, the energy dispersion can be expressed as

$$\varepsilon(\boldsymbol{k}) = \mu\sqrt{P + \nu\sqrt{Q}}, \tag{33}$$

with P and Q being the following:

$$\begin{aligned} P &= M^2 + U^2 + \tfrac{1}{2}\lambda_R^2 + v^2k^2; \\ Q &= \lambda_R^4/4 + v^2k^2\lambda_R^2 + 4v^2k^2M^2 - 2\eta MU\lambda_R^2 + 4M^2U^2, \end{aligned}$$

where $\mu = \pm 1$ stands for the conduction (+) and valence (−) bands; $\nu = \pm 1$ denotes the spin chirality. By imposing $k = 0$, the bulk band gap Δ at valleys K and K' can be determined to be

$$\Delta = 2|M - \eta U|, \tag{34}$$

which indicates that at valley K (i.e., $\eta = +1$), along with the increasing of the staggered AB sublattice potential U from zero, the bulk band gap Δ first decreases; at a critical $M = U$ point, the bulk gap is completely closed; when U further increases to be larger than M, a finite bulk gap reopens, indicating a topological phase transition. However, at the other valley K' (i.e., $\eta = -1$), the bulk gap Δ always increases and does not experience a topological phase transition. The different bulk band gap responses at K and K' are consistent with the tight-binding result discussed in Ref. 18.

For a small staggered AB sublattice potential U, the system is in the quantum anomalous Hall phase: Both valleys induce the same unit topological charge $\mathcal{C}_K = \mathcal{C}_{K'} = 1$. As long as the bulk gap is not completely closed at both K and K', the system should always belong to the quantum anomalous Hall phase. When $U > M$, a topological phase transition occurs at valley K, indicating a band inversion with Chern number becoming $\mathcal{C}_K = -1$. Since the topology at the valley K' always stays the same, i.e., $\mathcal{C}_{K'} = 1$, the total Chern number vanishes with $\mathcal{C} = \mathcal{C}_K + \mathcal{C}_{K'} = 0$. But the difference of Chern numbers at K and K' results in a quantum valley Hall phase with valley Chern number $\mathcal{C}_v = (\mathcal{C}_K - \mathcal{C}_{K'})/2 = 1$. Though the resulting new phase is the same as that in a gated bilayer graphene in the presence of Rashba spin-orbit coupling and exchange field,[11] the major difference is that the bulk gaps at K and K' are simultaneously closed at some critical parameters.[19]

In a gated bilayer graphene, when only the Rashba spin-orbit coupling is applied, the system experiences a topological phase transition from a quantum valley Hall phase to a two-dimensional strong topological insulator phase through tuning the gate bias between top and bottom layers.[20] It is natural to hope that a similar topological insulator phase can be realized by considering staggered AB sublattice potential and Rashba spin-orbit coupling in single-layer graphene, since staggered AB sublattice potential plays a similar role in breaking the out-of-plane inversion symmetry as the gate bias in bilayer graphene. However, we show that this is not the case. From Eq. (34), one can find that the bulk band gap is only dependent on the staggered AB sublattice potential U and the exchange field M but independent of the Rashba spin-orbit coupling strength. Thus, it is obvious that the resulting bulk gap in the absence of exchange would be a constant for any Rashba spin-orbit coupling strength at a fixed staggered potential U. This signals that the topological insulator state cannot

be achieved in single-layer graphene through tuning Rashba spin-orbit coupling.

B. Intrinsic spin-orbit coupling

Since the spin-orbit coupling (Rashba or intrinsic) in pristine graphene is very weak, one has to employ external means to enhance it. Recent *ab initio* studies reported that a better approach to enlarge the Rashba spin-orbit coupling is via doping low-concentration $3d$ or $5d$ transition-metal atoms on the hollow adsorption sites.[12,13] Though we only prefer the Rashba type spin-orbit coupling, the enhancement of the intrinsic one is unavoidable.[21] In the presence of intrinsic spin-orbit coupling, Rashba spin-orbit coupling, and exchange field, the continuum Hamiltonian is written as

$$H(\boldsymbol{k}) = h_0(\boldsymbol{k}) + h_R(\boldsymbol{k}) + h_{SO}(\boldsymbol{k}) + h_M(\boldsymbol{k}). \tag{35}$$

Through diagonalizing Eq. (35) at $\boldsymbol{k} = 0$, the energy spectrum at K can be expressed as

$$\begin{aligned}
\varepsilon_1^K &= +M + \lambda_{SO};\\
\varepsilon_2^K &= -M + \lambda_{SO};\\
\varepsilon_3^K &= +\sqrt{M^2 + \lambda_R^2} - \lambda_{SO};\\
\varepsilon_4^K &= -\sqrt{M^2 + \lambda_R^2} - \lambda_{SO}.
\end{aligned}$$

And the corresponding energy spectra at K' are

$$\begin{aligned}
\varepsilon_1^{K'} &= +\sqrt{M^2 + \lambda_R^2} + \lambda_{SO};\\
\varepsilon_2^{K'} &= +M - \lambda_{SO};\\
\varepsilon_3^{K'} &= -\sqrt{M^2 + \lambda_R^2} + \lambda_{SO};\\
\varepsilon_4^{K'} &= -M - \lambda_{SO}.
\end{aligned}$$

In general, the strength of the adatom-induced intrinsic spin-orbit coupling is an order of magnitude smaller than the induced Rashba strength, i.e., $\lambda_{SO} \ll \lambda_R$, and the exchange field is often lager than the Rashba spin-orbit coupling strength. Therefore, the resulting bulk band gaps at K and K' are

$$\Delta_K = \varepsilon_1^K - \varepsilon_2^K = 2M; \tag{36}$$

$$\Delta_{K'} = \varepsilon_2^{K'} - \varepsilon_4^{K'} = 2M. \tag{37}$$

This indicates that the bulk gaps at K and K' are only dependent on M. As long as $\lambda_{SO} \ll \lambda_R$, the quantum anomalous Hall phase would be robust against the weak intrinsic spin-orbit interaction.

From the theoretical point of view, if the intrinsic term is comparable with λ_R and M or even larger, the band gaps at K and K' are modified to be

$$\Delta_K = \left|\varepsilon_3^K - \varepsilon_2^K\right| = \left|\sqrt{M^2 + \lambda_R^2} + M - 2\lambda_{SO}\right|; \tag{38}$$

$$\Delta_{K'} = \left|\varepsilon_2^{K'} - \varepsilon_3^{K'}\right| = \left|\sqrt{M^2 + \lambda_R^2} + M - 2\lambda_{SO}\right|. \tag{39}$$

Therefore, at $\lambda_{SO} = (\sqrt{M^2 + \lambda_R^2} + M)/2$, the bulk band gap completely closes at both K and K'. And it enters a new phase with vanishing Chern number $\mathcal{C} = 0$ when the intrinsic spin-orbit coupling λ_{SO} further increases. Due to the presence of the exchange field M, the time-reversal symmetry is broken. Thus, it is no longer an intrinsic spin-orbit coupling-induced two-dimensional topological insulator.[14] In a recent paper, it has been reported that this new phase is a time-reversal-symmetry-broken quantum spin Hall phase.[22]

V. THEORY OF METAL ADSORPTION ON 3 × 3 AND 4 × 4 SUPERCELLS OF GRAPHENE

In the previous sections, we have assumed that all involved parameters are uniformly distributed on each atomic site of the graphene sheet. However, in a more realistic graphene sample, the atom dopants are usually adsorbed on graphene with a low concentration to avoid the direct transport through dopants themselves. For example, the mostly adopted systems in the *ab initio* study are 3×3, 4×4, 5×5, and 7×7 supercells of graphene. For 3×3 supercells, valleys K and K' are coupled to the Γ point resulting in the mixtures of valleys, but in the last three kinds of supercells valleys K and K' are separated and well-defined to be good quantum numbers. Therefore, in the following discussion we only consider two representing 3×3 and 4×4 supercells of graphene using the tight-binding methods.

There are three highly possible adsorption points in graphene: top, bridge, and hollow.[12,23] In Ref. 12, we have shown that only the hollow-site adsorption can open a nontrivial bulk gap to achieve the quantum anomalous Hall state. An obvious characteristic of this kind of adsorption is that the induced effects are nonuniformly distributed in the supercell; i.e., the six nearest carbon atoms under the metal adatom experience the largest exchange field M and Rashba spin-orbit coupling t_R, while for the other carbon atoms the longer the distance from the adsorption site, the smaller the induced interactions. Another most important term arising from the adsorption is the crystal field stabilization energy V_0 (also known as on-site energy), which is the main factor coupling valleys K and K' in the 3×3 supercell of graphene when Rashba and exchange effects are absent.

In Fig. 3 we schematically plot the 4×4 (a) and 3×3 (b) supercells of graphene. To emphasize the inhomogeneity, we only consider the externally induced effects (t_R, M, and V_0) on the six highlighted atomic sites of the supercells, while the remaining atomic sites are modeled as a pristine graphene. In our simulation, the effective tight-binding Hamiltonian is the same as Eq. (1) by setting $t_{SO} = 0$.

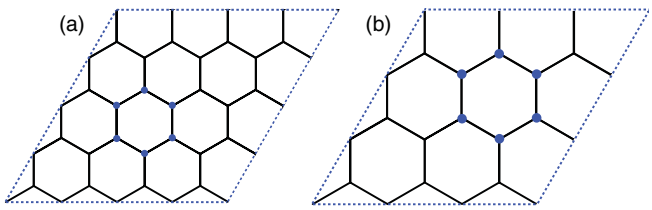

FIG. 3. (Color online) Schematic plot of (a) 4×4 and (b) 3×3 supercells of graphene. On-site crystal field potential, Rashba spin-orbit coupling, and exchange field are only considered on the highlighted sites.

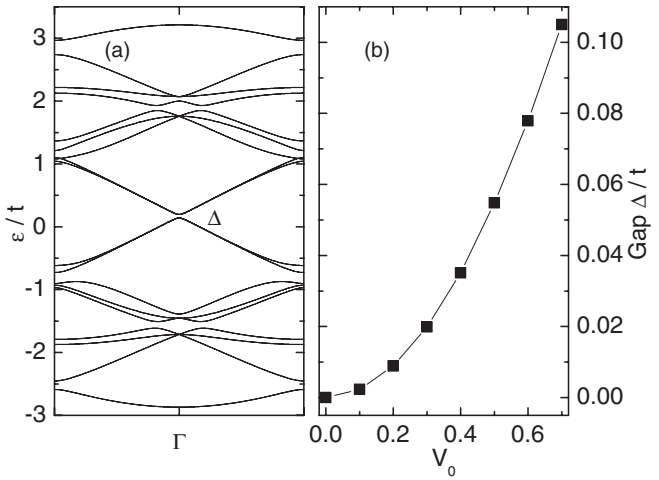

FIG. 4. (a) Bulk band structure of the 3×3 supercell of graphene in the presence of only on-site potential $V_0/t = 0.50$. A band gap Δ opens at the Γ point. (b) Bulk gap Δ quadratically increases as a function of V_0.

A. 3 × 3 supercell of graphene

Figure 4 plots the bulk band structure of the 3×3 supercell of graphene in the presence of only on-site potential and the resulting gap dependence as a function of the on-site potential. One can observe that a trivial band gap Δ opens at the Γ point [see Fig. 4(a)], and the opened band gap increases quadratically as a function of the on-site potential strength V_0. This confirms that it is the adsorption-induced on-site potential that couples valleys K and K' to open a band gap, consistent with the *ab initio* calculation result in Fig. 6 of Ref. 12.

When the exchange field M is further included, the bulk gap first decreases due to the relative shift between the spin-up polarized valence band and the spin-down polarized conduction band [see Fig. 5(a)]. For even larger M as shown in Fig. 5(b), one can observe that the gap is completely closed and the bands with opposite spin polarization cross.

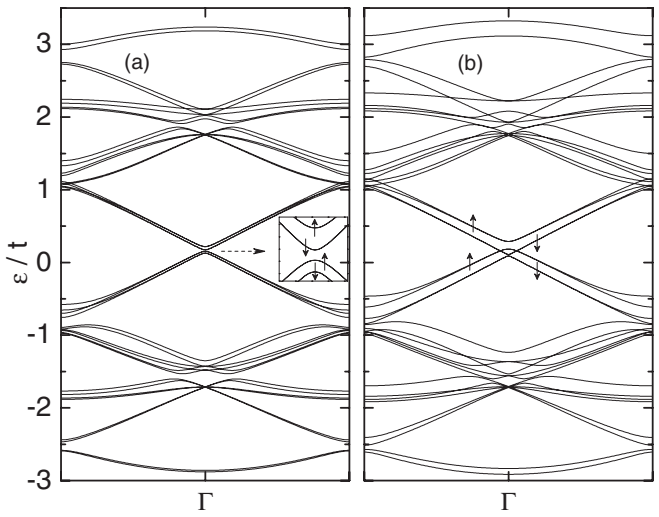

FIG. 5. Bulk band structure of the 3×3 supercell of graphene in the presence of on-site potential $V_0/t = 0.50$ and exchange field M. (a) $M/t = 0.05$, (b) $M/t = 0.20$. $\uparrow$ and $\downarrow$ denote up and down spin polarization.

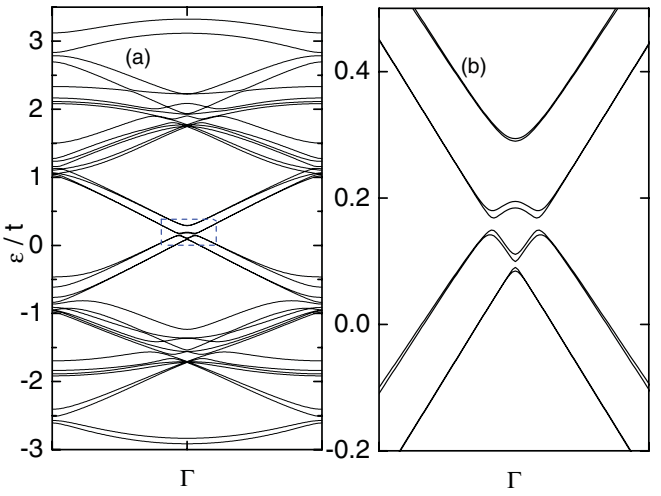

FIG. 6. (Color online) (a) Bulk band structure of the 3×3 supercell of graphene in the presence of on-site potential $V_0/t = 0.50$, exchange field $M/2 = 0.20$, and Rashba spin-orbit coupling $t_R/t = 0.05$. (b) The magnification of the band gap selected by the dashed square.

If Rashba spin-orbit coupling is considered in addition to the exchange field, we find that for small exchange field since the original band gap from on-site potential does not close, and the not-so-large Rashba spin-orbit coupling can only further reduce the band gap. However, for large exchange field, the situation becomes completely different; i.e., the Rashba spin-orbit coupling opens a new band gap at the band-crossing points as shown in Fig. 6.

To explore the nontrivial topology of the newly formed insulating phase, we plot the total Berry curvature distribution $\Omega(k_x, k_y)$ of the occupied valence bands below the gap in Fig. 7. One can find that the nonzero Berry curvatures are mainly

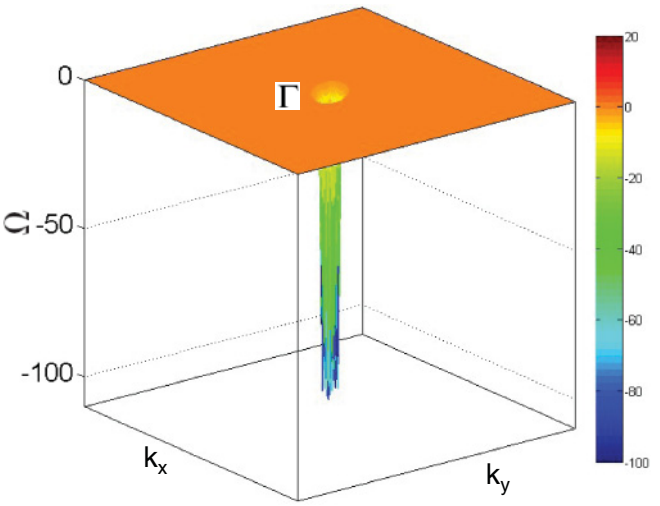

FIG. 7. (Color online) Total Berry curvature distribution Ω in the momentum space of the occupied valence bands below the band gap. Only those around the Γ point are nonzero and share the same negative sign.

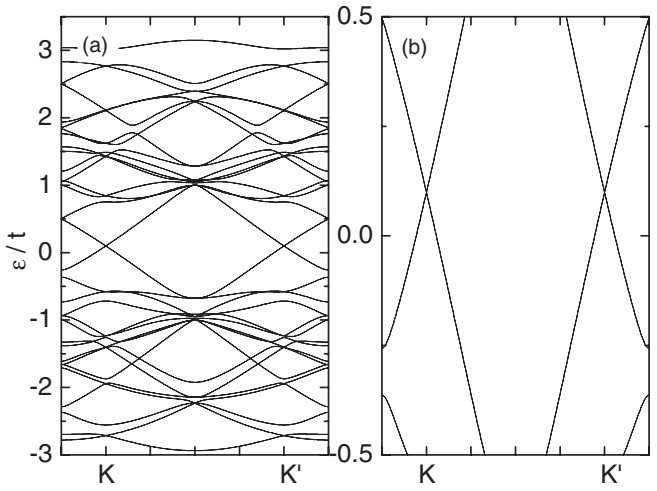

FIG. 8. (a) Bulk band structure of the 4×4 supercell of graphene in the presence of on-site potential $V_0/t = 0.50$. (b) Magnification of bands near the Dirac crossing point. No gap opens at K and K'.

located around the Γ point and share the same negative sign, suggesting a nonzero Chern number. Through an integration of Berry curvatures over the first Brillouin zone, the Chern number is calculated to be $\mathcal{C} = 2$.

Thus far, we can conclude that in the 3×3 supercells of graphene, the prerequisite to realize the quantum anomalous Hall effect is that the exchange field should be large enough to close the trivial band gap arising from the crystal field stabilization energy V_0. To our surprise, a separate work[24] proves that the randomness of the adsorption sites can exponentially diminish the trivial band gap determined by crystal field stabilization energy. This information manifests the high possibility of engineering the long-sought quantum anomalous Hall state in graphene through adsorbing random magnetic atoms.

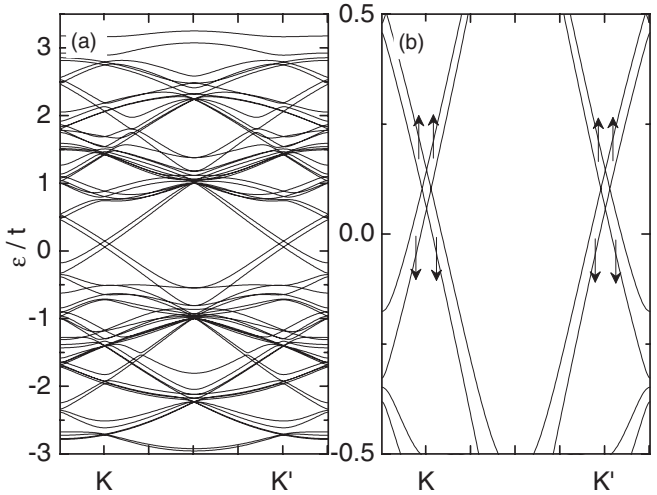

FIG. 9. (a) Bulk band structure of the 4×4 supercell of graphene in the presence of on-site potential $V_0/t = 0.50$ and exchange field $M/t = 0.20$. (b) Magnification of bands near the Dirac crossing point. Arrows are used to denote the up and down spin polarizations.

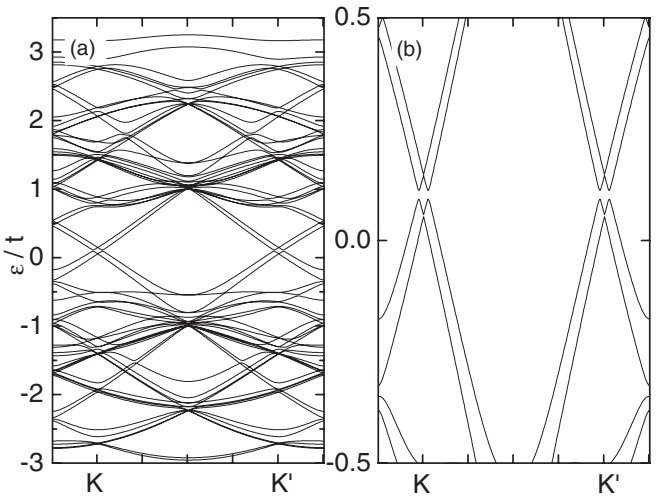

FIG. 10. (a) Bulk band structure of the 4×4 supercell of graphene in the presence of on-site potential $V_0/t = 0.50$, exchange field $M/t = 0.20$, and Rashba spin-orbit coupling $t_R/2 = 0.05$. (b) Magnification of bands near the Dirac crossing point. Bulk band gaps open at K and K'.

B. 4 × 4 supercell of graphene

Let us now study the 4×4 supercell of graphene case. Figure 8(a) plots the whole bulk band structure of the 4×4 supercell of graphene in the presence of only on-site potential V_0, and Fig. 8(b) magnifies the bands at the low-energy region. One can observe that the bands at K and K' exhibit linear Dirac-type dispersion without opening a band gap, which is completely different from the result of the 3×3 supercell of graphene. Comparing with the band structure of the pristine graphene, one can find that the bands at the low-energy regime are similar except for a Fermi-level shifting.

As shown in Fig. 9, when the exchange field is further considered, the doubly degenerate bands become spin split with spin-up bands upward shifting and spin-down bands downward shifting. This resembles the spin-split of graphene in the presence of uniformly distributed exchange field.[10]

Figure 10 plots the bulk band structure of the 4×4 supercell of graphene in the presence of on-site energies, exchange field, and Rashba spin-orbit coupling. One can observe that the Rashba spin-orbit coupling term opens a gap at the spin-up and spin-down band-crossing points near valleys K and K'. This gap formation should be nearly the same as that pointed out in Ref. 10. Therefore, the corresponding Chern number should be $\mathcal{C} = 2$. These tight-binding band structures reproduce the *ab initio* band structures demonstrated in Ref. 12.

VI. CONCLUSIONS

In this paper, we discuss the physical origins of the formation of the quantum anomalous Hall effect in graphene due to the presence of Rashba spin-orbit coupling λ_R and exchange field M using a continuum model. We show that in the limit of $M/\lambda_R \gg 1$, the quantization of the Hall conductance arises from skyrmions carried by the real-spin textures and merons carried by AB sublattice pseudospin

textures at K and K'; in the other limit $\lambda_R/M \gg 1$, the four-band low-energy Hamiltonian is reduced to an extended Haldane model, giving rise to a nonzero Chern number $\mathcal{C} = 1$ at either K or K'.

We demonstrate that the quantum anomalous Hall phase is robust against weak staggered AB sublattice potential U or intrinsic spin-orbit coupling λ_{SO}. In the presence of a moderate staggered AB sublattice potential, the system undergoes a phase transition from a quantum anomalous Hall phase to a quantum valley Hall phase if $U > M$. Alternatively, when a larger intrinsic spin-orbit coupling is applied, graphene in a quantum anomalous Hall phase transitions to a time-reversal-symmetry-broken quantum spin Hall phase[22] at $\lambda_{SO} = (\sqrt{M^2 + \lambda_R^2} + M)/2$.

Using a tight-binding model Hamiltonian, we reproduce all the *ab initio* band structures[12] (at the low energy level) of doping magnetic atoms on the hollow site of the 3×3 and 4×4 supercells of graphene by considering the on-site energy (crystal field stabilization energy), exchange field, and Rashba spin-orbit coupling on only a circle of six atomic sites, and explain the formations of the quantum anomalous Hall state in the 3×3 and 4×4 supercells of graphene. For the 3×3 supercell of graphene, we show that the crystal field stabilization energy is crucial to couple valleys K and K' to open a trivial bulk band gap at the Γ point in the absence of exchange field and Rashba spin-orbit coupling. We also find that only when the exchange field is large enough to close the trivial band gap from the crystal field stabilization energy, a nontrivial bulk band gap exhibiting the quantum anomalous Hall effect can be opened due to the presence of Rashba spin-orbit coupling. For the 4×4 supercell of graphene, due to the separation of valleys, no band gap opens when only the crystal field stabilization energy is present. When the exchange field and Rashba spin-orbit coupling are considered simultaneously, the physical mechanism to open a bulk gap is exactly the same as that in the presence of uniformly distributed parameters.[10] Recently, it was found that interaction-controlled pseudospin can also lead to zero-field Hall effect.[25]

ACKNOWLEDGMENTS

Z.Q. was supported by the NSF (Grant No. DMR 0906025) and the Welch Foundation (Grant No. F-1255). Q.N. was supported by the DOE (Grant No. DE-FG03-02ER45958, Division of Materials Science and Engineering) and the Texas Advanced Research Program. H.J. was supported by the CPSF (Grants No. 20100480147 and No. 201104030). Y.Y. was supported by the NSF of China (Grants No. 10974231 and No. 11174337) and the MOST Project of China (Grant No. 2011CBA00100).

[1] T. Ando, K. Matsumoto, and Y. Uemura, J. Phys. Soc. Jpn. **39**, 279 (1975); K. Klitzing, G. Dorda, and M. Pepper, Phys. Rev. Lett. **45**, 494 (1980).

[2] D. J. Thouless, M. Kohmoto, M. P. Nightingale, and M. den Nijs, Phys. Rev. Lett. **49**, 405 (1982).

[3] M. Kohmoto, Ann. Phys. (NY) **160**, 343 (1985).

[4] D. Xiao, M.-C. Chang, and Q. Niu, Rev. Mod. Phys. **82**, 1959 (2010).

[5] F. D. M. Haldane, Phys. Rev. Lett. **61**, 2015 (1988).

[6] C.-X. Liu, X.-L. Qi, X. Dai, Z. Fang, and S.-C. Zhang, Phys. Rev. Lett. **101**, 146802 (2008).

[7] M. Onoda and N. Nagaosa, Phys. Rev. Lett. **90**, 206601 (2003).

[8] C. Wu, Phys. Rev. Lett. **101**, 186807 (2008); Y. P. Zhang and C. W. Zhang, Phys. Rev. B **84**, 085123 (2011).

[9] R. Yu, W. Zhang, H.-J. Zhang, S.-C. Zhang, X. Dai, and Z. Fang, Science **329**, 61 (2010); H. Jiang, Z. H. Qiao, H. W. Liu, and Q. Niu, Phys. Rev. B **85**, 045445 (2012).

[10] Z. H. Qiao, S. A. Yang, W. X. Feng, W.-K. Tse, J. Ding, Y. G. Yao, J. Wang, and Q. Niu, Phys. Rev. B **82**, 161414(R) (2010).

[11] W.-K. Tse, Z. H. Qiao, Y. G. Yao, A. H. MacDonald, and Q. Niu, Phys. Rev. B **83**, 155447 (2011).

[12] J. Ding, Z. H. Qiao, W. X. Feng, Y. G. Yao, and Q. Niu, Phys. Rev. B **84**, 195444 (2011).

[13] H. B. Zhang, C. Lazo, S. Blügel, S. Heinze, and Y. Mokrousov, Phys. Rev. Lett. **108**, 056802 (2012).

[14] C. L. Kane and E. J. Mele, Phys. Rev. Lett. **95**, 146802 (2005); **95**, 226801 (2005).

[15] D. N. Sheng, Z. Y. Weng, L. Sheng, and F. D. M. Haldane, Phys. Rev. Lett. **97**, 036808 (2006); L. Sheng, D. N. Sheng, C. S. Ting, and F. D. M. Haldane, *ibid.* **95**, 136602 (2005).

[16] T. H. R. Skyrme, Nucl. Phys. **31**, 556 (1962); X. Z. Yu *et al.*, Nature (London) **465**, 901 (2010).

[17] M. Ezawa, Phys. Rev. B **83**, 100408(R) (2011); K. Moon, H. Mori, K. Yang, S. M. Girvin, A. H. MacDonald, L. Zheng, D. Yoshioka, and S. C. Zhang, *ibid.* **51**, 5138 (1995); A. Petković and M. V. Milovanović, Phys. Rev. Lett. **98**, 066808 (2007).

[18] Y. X. Xing, L. Zhang, and J. Wang, Phys. Rev. B **84**, 035110 (2011).

[19] Z. H. Qiao, W.-K. Tse, H. Jiang, X. Li, and Q. Niu (unpublished).

[20] Z. H. Qiao, W.-K. Tse, H. Jiang, Y. G. Yao, and Q. Niu, Phys. Rev. Lett. **107**, 256801 (2011).

[21] C. Weeks, J. Hu, J. Alicea, M. Franz, and R. Q. Wu, Phys. Rev. X **1**, 021001 (2011).

[22] Y. Y. Yang, Z. Xu, L. Sheng, B. G. Wang, D. Y. Xing, and D. N. Sheng, Phys. Rev. Lett. **107**, 066602 (2011).

[23] K. T. Chan, J. B. Neaton, and M. L. Cohen, Phys. Rev. B **77**, 235430 (2008).

[24] H. Jiang, Z. H. Qiao, H. W. Liu, J. R. Shi, and Q. Niu (unpublished).

[25] M. Trushin and J. Schliemann, Phys. Rev. Lett. **107**, 156801 (2011).